1-11-2012

Can morphology tailoring improve the open circuit voltage of organic solar cells?

Biswajit Ray
Purdue University - Main Campus, ray0@purdue.edu

M. S. Lundstrom
Purdue University School of Electrical Engineering

Muhammad A. Alam
Birck Nanotechnology Center, Purdue University

Ray, Biswajit; Lundstrom, M. S.; and Alam, Muhammad A., "Can morphology tailoring improve the open circuit voltage of organic solar cells?" (2012). *Birck and NCN Publications.* Paper 852.
http://dx.doi.org/10.1063/1.3672221

AIP | Applied Physics Letters

Can morphology tailoring improve the open circuit voltage of organic solar cells?

Biswajit Ray, Mark S. Lundstrom, and Muhammad A. Alam

Citation: Appl. Phys. Lett. **100**, 013307 (2012); doi: 10.1063/1.3672221
View online: http://dx.doi.org/10.1063/1.3672221
View Table of Contents: http://apl.aip.org/resource/1/APPLAB/v100/i1
Published by the American Institute of Physics.

Can morphology tailoring improve the open circuit voltage of organic solar cells?

Biswajit Ray,[a] Mark S. Lundstrom, and Muhammad A. Alam[b]
School of Electrical and Computer Engineering, Purdue University, West Lafayette, Indiana 47906, USA

(Received 7 June 2011; accepted 22 November 2011; published online 5 January 2012)

While the effect of interfacial morphology on the short circuit current (I_{SC}) of organic photovoltaic devices (OPVs) is well known, its impact on open circuit voltage (V_{OC}) and fill-factor (FF) are less clear. Since the output power of a solar cell $P_{out} = I_{SC}V_{OC}FF$, such understanding is critical for designing high-performance, morphology-engineered OPVs. In this letter, we provide an explicit analytical proof that any effort to radically improve V_{OC} by tailoring bulk heterojunction morphology is futile, because any increase in I_{SC} due to larger interface area is counterbalanced by corresponding increase in recombination current, so that the upper limit of V_{OC}^{BHJ} cannot exceed that of the corresponding planar heterojunction devices, i.e., $V_{OC}^{BHJ} \leq V_{OC}^{PHJ}$. We discuss the implication of this V_{OC}-constraint on the efficiency optimization of organic solar cells. © *2012 American Institute of Physics*. [doi:10.1063/1.3672221]

With the promise of low cost, high throughput, and flexible devices, the organic photovoltaic (OPV) cell is currently a topic of active interest. Historically, the first OPV cell was based on planar heterojunction (PHJ) device geometry,[1] consisting of two organic semiconductors called donor (D) and acceptor (A) stacked on top of each other. Photo-current in such OPV devices depends on the collection of photo-generated excitons, which require a heterojunction to dissociate into charge carriers. Thus, in PHJ-OPVs, only a fraction of the excitons, generated within a diffusion length ($L_{ex} \sim 10$ nm) of the heterojunction, can contribute to photocurrent (Fig. 1(a)). Since the junction area (A_{PHJ}) of PHJ-OPV is small, so is short circuit current $I_{SC}^{PHJ} \propto G_{ex}L_{ex}A_{PHJ}$, where G_{ex} is the spatially-averaged rate of photo-generation of excitons. This problem of low I_{SC}^{PHJ} was later solved by the elegant concept of the solution-processed bulk heterojunction (BHJ),[2] where the junction between the donor and acceptor material is distributed randomly throughout the volume of the cell. With the distributed large interfacial area ($A_{BHJ} \gg A_{PHJ}$), BHJ morphology enables exciton harvesting throughout the active volume with internal quantum efficiency approaching 100%.[3] This success has inspired various theoretical and experimental approaches (e.g., rod-coil co-polymer,[4] nano-imprint,[5] and templating[6]) to optimize morphology for maximum OPV efficiency. We will refer to all these devices collectively as BHJ-OPV.

Even though the BHJ-OPV improves I_{SC}, remarkably its morphology does not seem to have much effect on V_{OC}.[7–9] Recent research is thus focused on understanding or improving the V_{OC} of BHJ cells.[10–14] There is a growing (empirical) consensus that the *maximum limit* of V_{OC} is a material dependent parameter, which is determined either by electrode work function difference[15,16] or by the HOMO-LUMO gap (ΔE_{HL}) between the donor and acceptor materials[10–12] or a combination thereof.[12,15] Analytical expressions for V_{OC} have also been derived,[17–19] e.g.,

$$qV_{OC} = (\Delta E_{HL} - E_B - \Delta_{low}) - n_r kTln\left[\frac{\gamma N_A N_D}{J_{ph}}\right]. \quad (1)$$

Here the first three terms in Eq. (1) gives the maximum limit of V_{OC} and the last term captures the influence of light intensity (J_{ph}) and recombination strength (γ). The other terms in Eq. (1) are E_B is the exciton binding energy, Δ_{low} is the effective barrier lowering (due to image charge) at the metal-organic interface, n_r is the diode ideality factor, and N_D (or N_A) is the effective density of states in donor (or acceptor). Equation (1), however, cannot differentiate between two devices with completely different morphologies, because the analytical models in the literature are derived either with the assumption of PHJ devices[17,18] or with effective intrinsic media[19] approximation, and hence contains no notion of morphology.

In this letter, we model V_{OC}^{BHJ} as an explicit function of integrated D/A interfacial area (A_{BHJ}), regardless of the process details (templating,[6] annealing,[20–23] etc.) or the geometry of the morphology (e.g., planar, random, or regular). Our

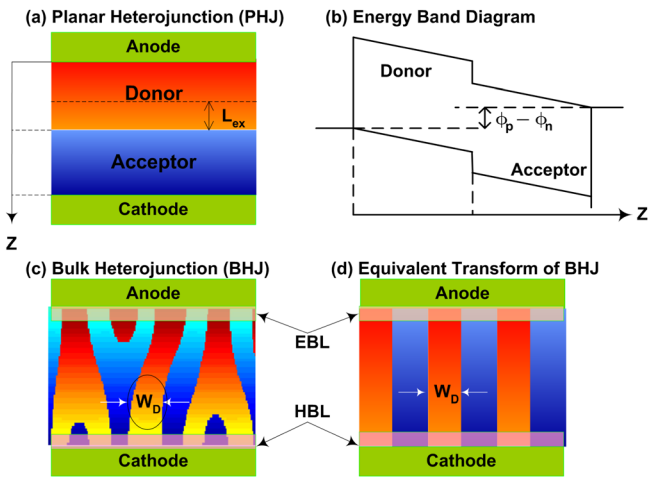

FIG. 1. (Color online) Structure of an organic solar cell. (a) PHJ based OPV cell. (b) The band diagram for PHJ cell at open circuit condition. (c) BHJ type OPV cell. The active layer morphology is generated by numerical simulation. W_D is the average domain size in the structure. (d) Equivalent geometrical transform of the complicated BHJ morphology. The width of the transformed rectangle is same as W_D of BHJ morphology. EBL and HBL are electron and hole blocking layers respectively.

[a]Electronic mail: biswajit.025@gmail.com.
[b]Electronic mail: alam@purdue.edu.

results establish the fundamental limit of V_{OC}^{BHJ} achievable by morphology engineering and highlight the trade-off between I_{SC}^{BHJ} and V_{OC}^{BHJ} in optimizing cell efficiency. We validate the analytical results by comparing with the full 3D numerical solution of the coupled exciton-electron-hole drift-diffusion transport within the phase segregated random morphology of BHJ-OPVs[4,24,25] and by consistently explaining a broad range of experimental observations.[20–23]

The short circuit current in a PHJ-OPV depends on the exciton diffusion flux at the interface (Fig. 1(a)). This flux is obtained by solving the 1D exciton diffusion equation subject to the boundary condition at the hetero-interface derived from Marcus theory.[26] Thus,

$$I_{SC}^{PHJ} \propto G_{ex} A_{PHJ} L_{ex} \tanh\left(\frac{T_D}{L_{ex}}\right), \tag{2}$$

where G_{ex} is the spatially-averaged exciton generation rate (for details, see Monestier *et al.*[27]) and $T_D (\equiv \eta_D T_{film})$ is the thickness of the donor layer (Fig. 1(a)) with η_D being the donor volume fraction in the active layer of film thickness T_{film}. For BHJ-OPVs, exciton diffusion depends on the complex 3D morphology characterized by A_{BHJ} (Fig. 1(c)). The 3D numerical solution of the exciton diffusion equation suggests that a simpler geometry can instead be used for flux calculation. This is done by transforming the complicated BHJ morphology to simpler rectangular geometry (keeping the volume of D/A phases fixed), so that the width of the transformed rectangle is defined by the average cluster size[28] W_D (Fig. 1(c)). The result for PHJ-OPVs (Eq. (2)) can now be used for this equivalent rectangular geometry to obtain

$$I_{SC}^{BHJ} \propto G_{ex} L_{ex} A_{BHJ} \tanh\left(\frac{\langle W_D \rangle}{2L_{ex}}\right) \equiv f_G(A_{BHJ}).I_{SC}^{PHJ}, \tag{3}$$

where $f_G(A_{BHJ})$ is a geometric amplification factor that encapsulates the improvement in short-current current of BHJ-OPVs over PHJ-OPVs. Note that f_G is exclusively determined by active layer geometry (using the fact that donor volume, $V_D = \eta_D T_{film} A_{PHJ} = \langle W_D \rangle A_{BHJ}/2$), i.e.,

$$f_G(A_{BHJ}) \equiv \left[\frac{A_{BHJ}}{A_{PHJ}}\right] \tanh\left(\frac{\eta_D T_{film} A_{PHJ}}{L_{ex} A_{BHJ}}\right) \Big/ \tanh\left(\frac{\eta_D T_{film}}{L_{ex}}\right).$$

PHJ-OPV can be viewed as a limiting case of BHJ-OPV, i.e., $A_{BHJ} = A_{PHJ}$, so that $f_G = 1$, i.e., there is no amplification. For a typical optimized morphology ($\langle W_D \rangle \cong 2L_{ex}$), $f_G \approx \frac{A_{BHJ}}{A_{PHJ}} > 1$, which explains the dramatic improvement of short-circuit current by BHJ-OPV morphology. See Fig. 2(a) for the plot of f_G as a function of A_{BHJ}.

At the open circuit condition, the recombination current (I_{rec}) cancels the photo-generation current (I_{SC}), making the net current zero. For PHJ-OPV, the recombination current at V_{OC} is given by

$$I_{rec}^{PHJ} \sim \gamma n(z_I^+) p(z_I^-) A_{PHJ} = \gamma n_{int}^2 exp\left[\frac{qV_{OC}^{PHJ}}{n_r kT}\right] A_{PHJ}, \tag{4}$$

where n_{int} is the intrinsic carrier concentration at the D-A interface, given by $n_{int}^2 = N_A N_D \exp\left(-\frac{\Delta E_{HL}}{kT}\right)$. Equation (4) follows from the fact that $n(z_I^+)p(z_I^-) = n_{int}^2 exp[q(\phi_p - \phi_n)/n_r kT]$, where $\phi_{n,p}$ is the electro-chemical potential of electron (n) and hole (p) at the interface. The zero current condition at V_{OC} implies constant electro-chemical potential throughout the device in a PHJ-OPV geometry, given the fact that carrier transport is unipolar in D/A regions (Fig. 1(b)). Thus, at open circuit condition $(\phi_p - \phi_n) = V_{OC}$.

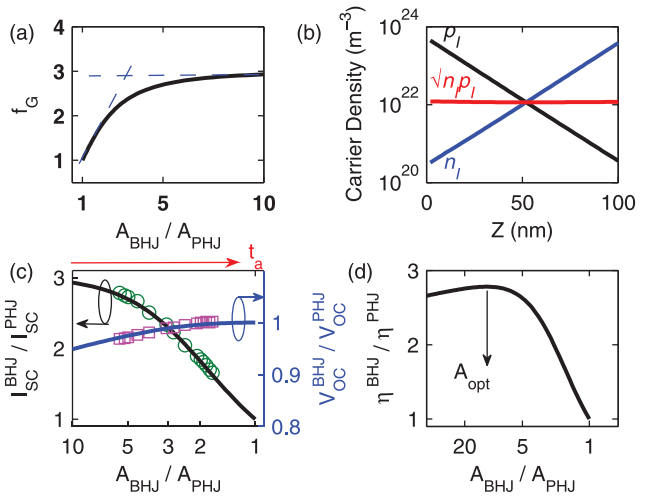

FIG. 2. (Color online) Validation of analytical model (solid line) with detailed numerical simulation (symbols). (a) The geometric amplification function $f_G(A_{BHJ})$ is plotted. Note that for $A_{BHJ} \gg A_{PHJ}$, the function f_G saturates to a fixed value given by $\eta_D T_{film}/L_{ex}$. (b) Interfacial carrier densities as a function of distance from anode to cathode are plotted. We note that product of the interfacial carrier densities remains essentially constant throughout the active volume. (c) Short circuit current (I_{SC}^{BHJ}) of BHJ cell normalized by short circuit current (I_{SC}^{PHJ}) of PHJ cell is plotted against total D-A interfacial area (A_{BHJ}), divided by PHJ cell area (A_{PHJ}). Open circuit voltage of BHJ cell (V_{OC}^{BHJ}) is also plotted against area of interface on the right hand side axis. (d) The η^{BHJ}/η^{PHJ} is plotted assuming same FF for both PHJ and BHJ cell.

A key observation from the 3D numerical simulation of carrier density inside the BHJ morphology (Fig. 1(c)) is that *regardless the complexity of the interfacial structure*, the $n_I p_I$ product (subscript "'I" stands for interfacial nodes) is a constant equal to $n_I p_I^{PHJ}$ throughout the BHJ-OPV (Fig. 2(b)). Therefore, the recombination current at V_{OC} is given by

$$I_{rec}^{BHJ} = \int\int \gamma n_I(z) p_I(z) dS(z) = \gamma n_{int}^2 exp\left[\frac{qV_{OC}^{BHJ}}{n_r kT}\right] A_{BHJ} \ . \tag{5}$$

This ability to evaluate the complex surface integral over arbitrary morphology as a trivial sum over interfacial area makes analytical calculation of V_{OC} possible. Equation (5) assumes that the minority carrier blocking layers (below the contacts) will prevent carrier recombination (or carrier escape) at the wrong metal-semiconductor contacts.

The expression of V_{OC}^{PHJ} is derived[17–19] from the condition of $I_{rec}^{PHJ}(V_{OC}) \sim I_{SC}^{PHJ}$, given the fact that the recombination at short circuit condition is generally negligible. Combining Eqs. (2) and (4), we find

$$V_{OC}^{PHJ} = \frac{n_r kT}{q} ln\left[\frac{I_{SC}^{PHJ}}{\gamma n_{int}^2 A_{PHJ}}\right].$$

With substitution of auxiliary relationships used in deriving Eq. (4), we find Eq. (1) for PHJ-OPV, as expected. The corresponding equation for V_{OC}^{BHJ} is (using Eqs. (3) and (5))

$$V_{OC}^{BHJ} = V_{OC}^{PHJ} + \frac{n_r kT}{q} ln\left[\left(\frac{A_{PHJ}}{A_{BHJ}}\right) f_G(A_{BHJ})\right], \tag{6}$$

where V_{OC}^{PHJ} contains all the D-A material specific parameters, while the second term involves explicit geometrical factors associated with BHJ-OPVs. Let us illustrate three cases associated with Eq. (6). (i) For PHJ device, $A_{BHJ} = A_{PHJ}$ ($f_G = 1$) and the second term in Eq. (6) vanishes, thereby establishing the upper limit of $V_{OC}^{BHJ} = V_{OC}^{PHJ}$. (ii) For a typical optimized BHJ cell, $f_G \approx A_{BHJ}/A_{PHJ}$ and hence the second term is negligible, making V_{OC}^{BHJ} almost independent of A_{BHJ}. Finally, (iii) for the very fine morphology with $A_{BHJ} \gg A_{PHJ}$, f_G becomes a constant much smaller than A_{BHJ}/A_{PHJ} (Fig. 2(a)), which makes the correction term in Eq. (6) negative, so that $V_{OC}^{BHJ} \leq V_{OC}^{PHJ}$ at the early stage of phase-segregation, consistent with the broad range of experimental results.[7–9]

To validate Eqs. (3) and (6) numerically, we simulate a series of random BHJ morphologies by phase field approach and extract the interfacial area A_{BHJ} directly from the simulated morphologies. The I_{SC} and V_{OC} for each such structure are simulated by solving the coupled transport equations (based on drift-diffusion formalism) for excitons, electrons, and holes. Details of the process-device simulation methodology are given in Ref. 25. Fig. 2(c) shows remarkably good agreement between numerical and analytical results over broad range of morphologies. Equations (3) and (6) also offer intuitive interpretation of several puzzling features of BHJ-OPVs observed during annealing (or thermal) experiments. Experimentally, it is well established that longer annealing reduces the I_{SC};[28,29] however, V_{OC} remains unchanged with anneal time. Equation (3) attributes the reduction of I_{SC} to the coarsening (Oswald ripening) of the phase-segregated morphology[28,29] and the reduction in total interfacial area (A_{BHJ}). This effect reduces the geometrical amplification factor and hence I_{SC}. Similarly, the counterintuitive insensitivity of V_{OC} with morphology coarsening is explained by Eq. (6). Since both the photocurrent, Eq. (3), and the recombination current, Eq. (5), are proportional to the interfacial area, V_{OC}^{BHJ}, which depends on the ratio of these two currents, remains insensitive to morphology evolution. Note that the single parameter (A_{BHJ}) description of the complex morphology[30] is obviously an approximation; the approach nonetheless allows us to establish the upper-limits of the OPV metrics and explain a number of counterintuitive features of the experiments in an intuitively simple manner (experimental trends are summarized in Ref. 31).

The results in Fig. 2(c) show that V_{OC}^{BHJ} decreases with higher interfacial area, while I_{SC}^{BHJ} shows the opposite trend. Since the power output of a solar cell $P_{out} = I_{SC}V_{OC}FF$, the optimal efficiency of the cell depends on the trade-off between I_{SC}^{BHJ} and V_{OC}^{BHJ}. In Fig. 2(d), we plot η^{BHJ}/η^{PHJ} (dashed line), assuming the same fill-factor for both PHJ and BHJ cell (in practice, the $FF^{BHJ} < FF^{PHJ}$ due to longer transport length and higher effective series resistance). The results show that the optimum efficiency is obtained ($A_{BHJ} \tilde{} 10A_{PHJ}$) as a balance between increasing $I_{SC}^{BHJ}(A_{BHJ})$, with (weakly) decreasing $V_{OC}^{BHJ}(A_{BHJ})$.

In summary, we have derived analytical expressions for the short circuit current and open circuit voltage as a function of the interfacial area of disordered BHJ solar cells to show that unlike I_{SC}^{BHJ}, V_{OC}^{BHJ} is relatively insensitive to the morphology and hence it cannot be radically improved by morphology-engineering. Equations (3) and (6) should find broad application in interpreting various OPV experiments and can eventually be used, for example, as process monitor of the evolution of interfacial area as a function of anneal time.

We gratefully acknowledge financial support from the DOE-ERFC at Columbia (No. DE SC0001085) and computational resources from NSF-NCN Center at Purdue (EEC 0228390).

[1]C. W. Tang, Appl. Phys. Lett. **48**, 183 (1986).
[2]G. Yu, J. Gao, J. C. Hummelen, F. Wudl, and A. J. Heeger, Science **270**, 1789 (1995).
[3]S. H. Park, A. Roy, S. Beaupre, S. Cho, N. Coates, J. S. Moon, D. Moses, M. Leclerc, K. Lee, and A. J. Heeger, Nat. Photonics **3**, 297 (2009).
[4]M. Shah and V. Ganesan, Macromolecules **43**, 543 (2010).
[5]Z. Fan, H. Razavi, J.-W. Do, A. Moriwaki, O. Ergen, Y.-L. Chueh, P. W. Leu, J. C. Ho, T. Takahashi, L. A. Reichertz, S. Neale, K. Yu, M. Wu, J. W. Ager, and A. Javey, Nat. Mater. **8**, 648 (2009).
[6]A. A. Gorodetsky, C.-Y. Chiu, T. Schiros, M. Palma, M. Cox, Z. Jia, W. Sattler, I. Kymissis, M. Steigerwald, and C. Nuckolls, Angew. Chem. Int. Ed. **49**, 7909 (2010).
[7]C. Uhrich, D. Wynands, S. Olthof, M. K. Riede, K. Leo, S. Sonntag, B. Maennig, and M. Pfeiffer, J. Appl. Phys. **104**, 043107–6 (2008).
[8]T. A. M. Ferenczi, J. Nelson, C. Belton, A. M. Ballantyne, M. Campoy-Quiles, F. M. Braun, and D. D. C. Bradley, J. Phys.: Condens. Matter **20**, 475203 (2008).
[9]A. L. Ayzner, C. J. Tassone, S. H. Tolbert, and B. J. Schwartz, J. Phys. Chem. C **113**, 20050 (2009).
[10]M. C. Scharber, D. Mühlbacher, M. Koppe, P. Denk, C. Waldauf, A. J. Heeger, and C. J. Brabec, Adv. Mater. **18**, 789 (2006).
[11]B. P. Rand, D. P. Burk, and S. R. Forrest, Phys. Rev. B **75**, 115327 (2007).
[12]M. F. Lo, T. W. Ng, T. Z. Liu, V. A. L. Roy, S. L. Lai, M. K. Fung, C. S. Lee, and S. T. Lee, Appl. Phys. Lett. **96**, 113303–3 (2010).
[13]H.-Y. Chen, J. Hou, S. Zhang, Y. Liang, G. Yang, Y. Yang, L. Yu, Y. Wu, and G. Li, Nat. Photonics **3**, 649 (2009).
[14]A. Tada, Y. Geng, Q. Wei, K. Hashimoto, and K. Tajima, Nat. Mater. **10**, 450 (2011).
[15]V. D. Mihailetchi, P. W. M. Blom, J. C. Hummelen, and M. T. Rispens, J. Appl. Phys. **94**, 6849 (2003).
[16]C. Zhang, S.-W. Tong, C.-Y. Jiang, E.-T. Kang, D. S. H. Chan, and C. Zhu, IEEE Trans. Electron Devices **57**, 397 (2010).
[17]D. Cheyns, J. Poortmans, P. Heremans, C. Deibel, S. Verlaak, B. P. Rand, and J. Genoe, Phys. Rev. B **77**, 165332 (2008).
[18]N. C. Giebink, G. P. Wiederrecht, M. R. Wasielewski, and S. R. Forrest, Phys. Rev. B **82**, 155305 (2010).
[19]L. J. A. Koster, V. D. Mihailetchi, R. Ramaker, and P. W. M. Blom, Appl. Phys. Lett. **86**, 123509–3 (2005).
[20]L. Zeng, C. W. Tang, and S. H. Chen, Appl. Phys. Lett. **97**, 053305–3 (2010).
[21]Y.-C. Huang, Y.-C. Liao, S.-S. Li, M.-C. Wu, C.-W. Chen, and W.-F. Su, Sol. Energy Mater. Sol. Cells **93**, 888 (2009).
[22]H. Kim, M. Shin, J. Park, and Y. Kim, IEEE Trans. Nanotechnol. **9**, 400 (2010).
[23]J. A. Renz, T. Keller, M. Schneider, S. Shokhovets, K. D. Jandt, G. Gobsch, and H. Hoppe, Sol. Energy Mater. Sol. Cells **93**, 508 (2009).
[24]G. A. Buxton and N. Clarke, Phys. Rev. B **74**, 085207 (2006).
[25]B. Ray, P. R. Nair, and M. A. Alam, Sol. Energy Mater. Sol. Cells **95**, 3287 (2011).
[26]R. A. Marcus, Rev. Mod. Phys. **65**, 599 (1993).
[27]F. Monestier, J.-J. Simon, P. Torchio, L. Escoubas, F. Flory, S. Bailly, R. de Bettignies, S. Guillerez, and C. Defranoux, Sol. Energy Mater. Sol. Cells **91**, 405 (2007).
[28]B. Ray and M. A. Alam, Appl. Phys. Lett. **99**, 033303–3 (2011).
[29]J. Jo, S.-S. Kim, S.-I. Na, B.-K. Yu, and D.-Y. Kim, Adv. Funct. Mater. **19**, 866 (2009).
[30]S. D. Oosterhout, M. M. Wienk, S. S. van Bavel, R. Thiedmann, L. Jan A. Koster, J. Gilot, J. Loos, V. Schmidt, and R. A. J. Janssen, Nat. Mater. **8**, 818 (2009).
[31]See supplementary material at http://dx.doi.org/10.1063/1.3672221 for experimental trends from literature.